PULMONARY FIBROSIS

Targeted inhibition of PI3 kinase/mTOR specifically in fibrotic lung fibroblasts suppresses pulmonary fibrosis in experimental models

Suraj U. Hettiarachchi[1], Yen-Hsing Li[1], Jyoti Roy[1], Fenghua Zhang[1], Estela Puchulu-Campanella[1], Spencer D. Lindeman[1], Madduri Srinivasarao[1], Konstantin Tsoyi[2,3], Xiaoliang Liang[2,3], Ehab A. Ayaub[2], Cheryl Nickerson-Nutter[4], Ivan O. Rosas[2,3], Philip S. Low[1]*

Idiopathic pulmonary fibrosis (IPF) is a lethal disease with an average life expectancy of 3 to 5 years. IPF is characterized by progressive stiffening of the lung parenchyma due to excessive deposition of collagen, leading to gradual failure of gas exchange. Although two therapeutic agents have been approved from the FDA for IPF, they only slow disease progression with little impact on outcome. To develop a more effective therapy, we have exploited the fact that collagen-producing myofibroblasts express a membrane-spanning protein, fibroblast activation protein (FAP), that exhibits limited if any expression on other cell types. Because collagen-producing myofibroblasts are only found in fibrotic tissues, solid tumors, and healing wounds, FAP constitutes an excellent marker for targeted delivery of drugs to tissues undergoing pathologic fibrosis. We demonstrate here that a low–molecular weight FAP ligand can be used to deliver imaging and therapeutic agents selectively to FAP-expressing cells. Because induction of collagen synthesis is associated with phosphatidylinositol 3-kinase (PI3K) activation, we designed a FAP-targeted PI3K inhibitor that selectively targets FAP-expressing human IPF lung fibroblasts and potently inhibited collagen synthesis. Moreover, we showed that administration of the inhibitor in a mouse model of IPF inhibited PI3K activation in fibrotic lungs, suppressed production of hydroxyproline (major building block of collagen), reduced collagen deposition, and increased mouse survival. Collectively, these studies suggest that a FAP-targeted PI3K inhibitor might be promising for treating IPF.

INTRODUCTION

Pathologic fibrosis involves the excessive deposition of fibrous tissue, primarily collagen, leading to tissue remodeling that interferes with normal organ function and ultimately leads to organ failure (*1*). Although virtually any tissue can experience pathologic fibrosis, the most commonly affected are the lungs, kidneys, liver, skin, heart, and bladder (*2*, *3*). Because of the difficulty in diagnosing these diseases, their total incidences have not been accurately recorded; however, it has been estimated that 30 to 40% of morbidity in developed countries is caused by their collective occurrence (*2*–*4*).

Idiopathic pulmonary fibrosis (IPF) arises from progressive fibrosis of the lungs that occurs primarily in individuals over the age of 50 and commonly results in death within 3 to 5 years of diagnosis (*5*–*7*). In the United States, IPF kills ~40,000 people/year (as many as breast cancer), with most treatment options focused on managing patient lifestyle and/or supplementing oxygen supply. Although two drugs, pirfenidone and nintedanib, have been approved for treatment of IPF, both provide only limited and inconsistent efficacy, primarily retarding disease progression but not leading to resolution of the pathology (*6*, *8*). Several kinase inhibitors have also been introduced into clinical trials; however, their inhibition of the targeted enzymes in healthy tissues has raised concerns regarding possible systemic toxicities (*6*, *9*, *10*). Although lung transplantation remains a final treatment option, survival is still often limited and the cost of lung transplantation is high compared with medical therapies.

To design a more effective treatment for IPF, we have explored a strategy to suppress activation of fibroblasts that cause unwanted fibrosis. In response to stimulation by key fibrogenic mediators such as transforming growth factor–β_1 (TGFβ_1), chemokine ligand 18 (CCL18), platelet-derived growth factor (PDGF), and other growth factors, fibroblasts can differentiate into myofibroblasts that oversynthesize collagen and other extracellular matrix proteins (*11*–*14*). These activated myofibroblasts can be distinguished from nonpathogenic fibroblasts by their expression of fibroblast activation protein (FAP), a membrane-spanning protein that is critical for collagen remodeling (*15*). Because FAP exhibits low to undetectable expression in most healthy cell types, with notable exceptions being cancer-associated fibroblasts and fibroblasts in tissues undergoing remodeling or repair (*15*–*23*), expression of FAP on myofibroblasts provides a molecular marker that can be exploited for the targeted delivery of drugs specifically to the subset of fibroblasts that causes fibrosis.

In this study, we describe the synthesis and use of a new FAP-specific targeting ligand for delivery of a phosphatidylinositol 3-kinase inhibitor (PI3Ki) to collagen-producing fibroblasts in fibrotic lung tissues. We demonstrate that our FAP-targeted PI3Ki can inhibit PI3K activity in both normal lung fibroblasts activated with TGFβ_1 and human IPF lung fibroblasts cultured in vitro. We further show that the FAP-targeted PI3Ki can suppress alpha smooth muscle actin (αSMA) expression (a marker of fibroblast activation), hydroxyproline production (a building block of collagen), collagen deposition, and development of lung fibrosis in a mouse model of experimental lung fibrosis induced by bleomycin administration. We finally document that the FAP-targeted PI3Ki has beneficial effects in lung slices from

[1]Department of Chemistry and Institute for Drug Discovery, Purdue University, West Lafayette, IN 47907, USA. [2]Division of Pulmonary and Critical Care Medicine, Brigham and Women's Hospital, Harvard Medical School, Boston, MA 02115, USA. [3]Pulmonary, Critical Care and Sleep Medicine, Baylor College of Medicine, Houston, TX 77030, USA. [4]Three Lakes Foundation, Northbrook, IL 60062, USA.
*Corresponding author. Email: plow@purdue.edu

patients with IPF. Our results suggest that the FAP-targeted PI3Ki warrants further scrutiny as a potential therapy for IPF.

RESULTS

Binding and uptake of FAP-targeted fluorescein by FAP-expressing human lung fibroblasts

To deliver drugs specifically to activated IPF lung myofibroblasts, we searched for an IPF-specific receptor and an associated targeting ligand that could be exploited for selective delivery of antifibrotic drugs to activated profibrotic fibroblasts. On the basis of reports in the literature that FAP is up-regulated in human IPF lung fibroblasts (*15*) but largely absent from all other cell types except cancer-associated fibroblasts and fibroblasts in tissues undergoing repair or remodeling, we digested both healthy and IPF human lung tissue and examined the resulting cell suspensions for expression of FAP. As shown in fig. S1, FAP is only expressed on lung fibroblasts and is strongly up-regulated in fibrotic tissue. We therefore concluded that FAP could be a good marker for selective delivery of therapeutics to the activated subset of fibroblasts in IPF lungs and proceeded with a search for a targeting ligand that would bind selectively to FAP. For this purpose, we used a FAP-specific ligand that had been previously designed for delivery of drugs to cancer-associated fibroblasts found in most solid tumors (*24*). To test the ability of this ligand to target drugs to myofibroblasts in fibrotic tissues, we linked the FAP targeting ligand (FAPL) to fluorescein (Fig. 1A, top structure) and examined its interaction with a stable human lung fibroblast cell line with FAP expression (HLF-FAP). As shown in the confocal micrographs of Fig. 1B, the fluorescent conjugate (FAPL-fluorescein) was found to bind HLF-FAP cells and rapidly internalize into Rab7a-expressing endosomes, resulting in a 7 ± 0.8-fold increase in FAPL-fluorescein fluorescence in Rab7a$^+$ endosomes between 5 and 30 min after addition. As further revealed in fig. S2, the same fluorescein conjugate was demonstrated to bind FAP with high affinity (K_D ~10 nM), and the binding could be largely prevented by coadministration of excess FAPL, confirming that binding was FAP specific. Last, as also revealed in fig. S2, binding of FAPL-fluorescein to human lung fibroblast (HLF) cells not transfected with FAP was minimal, suggesting that induction of FAP expression was required for FAPL-fluorescein binding. Together, these data suggest that FAPL constitutes an attractive candidate for specific targeting of drugs to myofibroblasts in fibrotic tissues.

To determine whether FAPL-mediated drug delivery can occur in a more IPF-relevant cell type, we next examined FAPL-fluorescein uptake by primary HLFs obtained from patients with IPF. As shown in Fig. 1C and fig. S3, FAPL-fluorescein binds 15 ± 1-fold greater than IPF lung fibroblasts (as confirmed by its colocalization with αSMA), whereas little uptake is seen by control fibroblasts obtained from human lung explants. These data indicate that the FAPL might be used to deliver attached drugs to human IPF myofibroblasts.

Design and synthesis of a PI3Ki for inhibition of collagen synthesis

To determine whether FAPL might be exploited to deliver an attached inhibitor of collagen synthesis into HLFs, we next scrutinized the literature for myofibroblast signaling pathways that have been

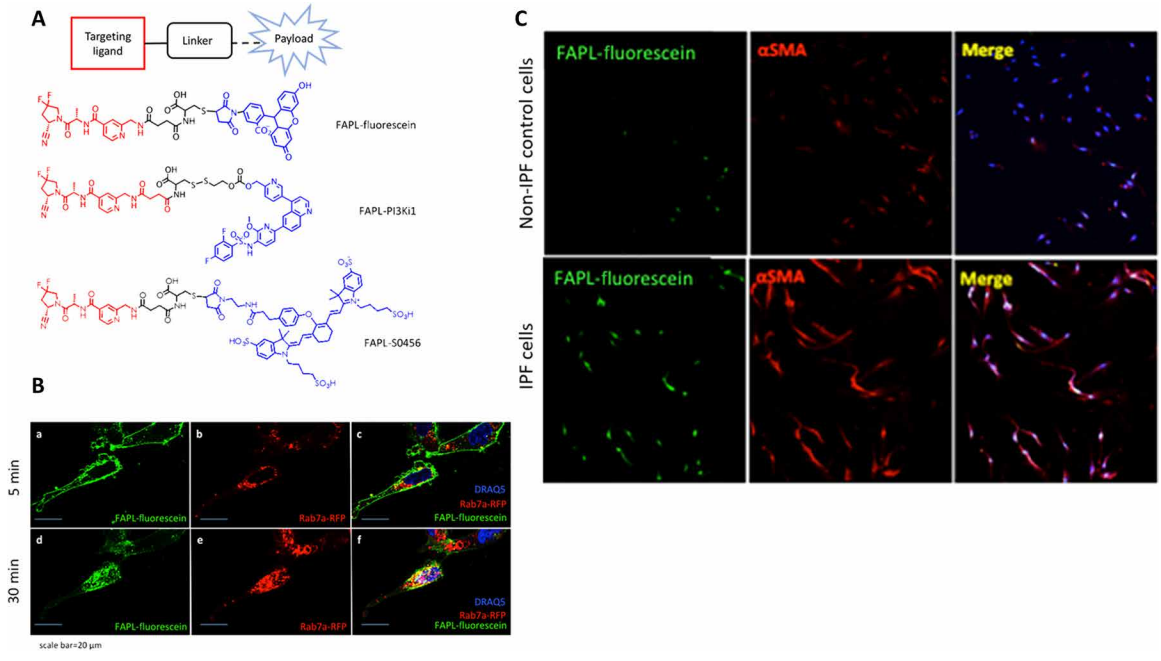

Fig. 1. FAPL-fluorescein binds and is internalized by a FAP-expressing human lung fibroblast cell line (HLF-FAP) and fibroblasts from a patient with IPF. (**A**) Structures of FAP ligand–targeted fluorescein (FAPL-fluorescein), PI3 kinase inhibitor (FAPL-PI3Ki1), and NIR dye (FAPL-S0456). (**B**) Live cell images of FAPL-fluorescein binding and internalization. Confocal microscopy of HLF-FAP cells expressing the late endosomal marker Rab7a-RFP incubated with FAPL-fluorescein and imaged 5 min (a to c) and 30 min (d to f) after FAPL-fluorescein addition. FAPL-fluorescein staining is shown in green, whereas Rab7a-RFP is shown in red. DRAQ5 nuclei stain is shown in blue. Colocalization of FAPL-fluorescein with Rab7a-RFP is shown in (c) and (f) (indicated in yellow). (**C**) Comparison of FAPL-fluorescein uptake by non-IPF (upper row) and IPF (lower row) human lung fibroblast. Binding of FAPL-fluorescein and expression of alpha smooth muscle actin (αSMA), a fibroblast activation marker, are shown in green and red, respectively. The merging of the two markers is shown in pink (right column).

shown to be required for collagen production/secretion. On the basis of reports that TGFβ$_1$ induction of collagen synthesis by IPF lung fibroblasts requires activation of PI3K (*25*, *26*), we undertook to design a PI3Ki that could be readily delivered into myofibroblasts with FAPL. Although omipalisib, a PI3Ki recently introduced into IPF clinical trials (*27*), lacked a functional group for conjugation to FAPL (Fig. 2A), we thought of developing a molecule similar to omipalisib that would retain its inhibitory potency with the addition of a functional group for conjugation to FAPL via a cleavable linker. The PI3Ki shown in Fig. 2B (PI3Ki1) contains the modified omipalisib, and the structure of its conjugate to FAPL is presented in Fig. 1A (middle structure). Figure 2C then shows how reduction of the disulfide bond connecting FAPL to PI3Ki1 within an intracellular reducing environment can trigger self-immolative release of the unmodified PI3Ki1 for inhibition of collagen synthesis. As shown in Fig. 2D (left), the difluorosulfonamide end of omipalisib is seen to fit well into the bottom of the catalytic site of PI3Kγ, allowing the quinoline end of the inhibitor to protrude into the aqueous space. However, as noted above, because the aqueous-exposed pyridazine cannot be derivatized with FAPL, we converted it into a pyridine-hydroxymethyl substituent, which was readily conjugated to FAPL. This pyridine-hydroxymethyl modification not only did not obstruct binding of the inhibitor to PI3K but also actually enhanced the affinity of the modified inhibitor (PI3Ki1) for PI3K (table S1).

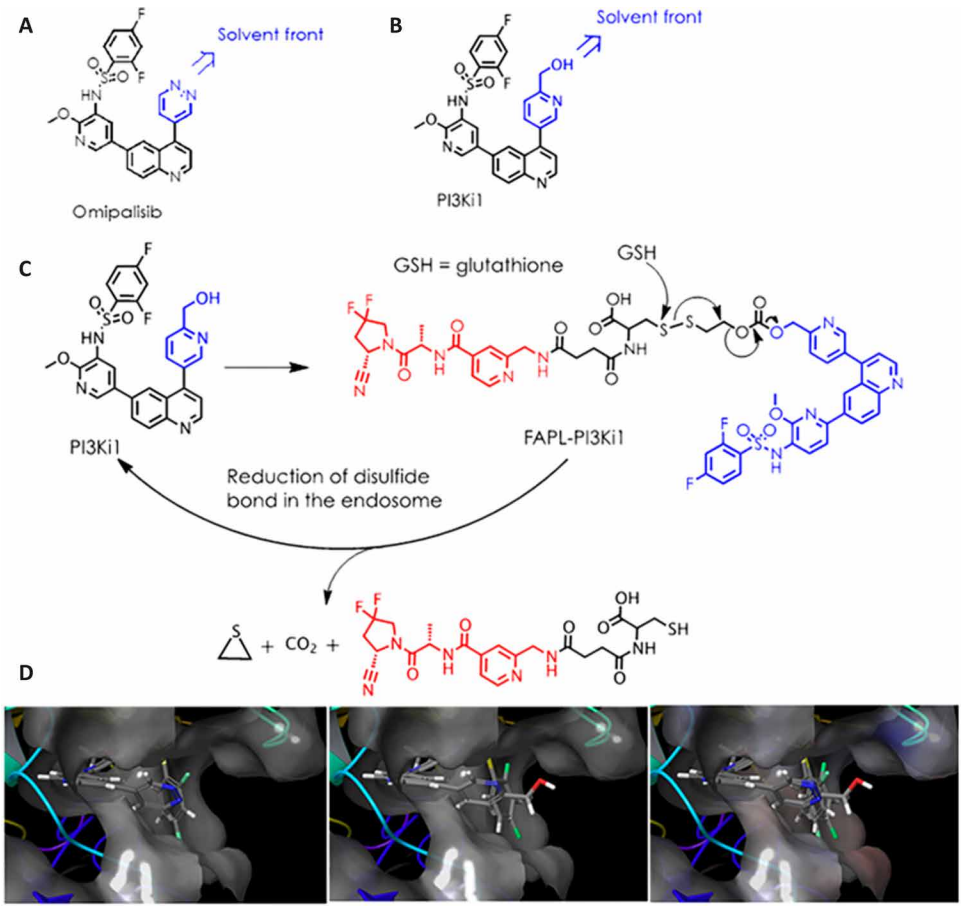

Fig. 2. Design of a derivatizable PI3Ki for use in FAP-targeted delivery to IPF fibroblasts. (**A**) Structure of omipalisib, a potent PI3Ki in human clinical trials. (**B**) Structure of the derivatizable analog of omipalisib, PI3Ki, for use in conjugation via a releasable linker to FAPL. (**C**) Schematic showing the release of PI3Ki upon cell entry. The reductive environment of the endosome cleaves the disulfide bond, triggering a self-immolative release of the free PI3Ki1. (**D**) Schrödinger Maestro docking of the pan-PI3K/mTOR inhibitor (omipalisib; left), pyridine-hydroxymethyl derivative of omipalisib (PI3Ki1; middle), and overlay of the two inhibitors (right) in the active site of PI3Kγ (PDB code: 3L08).

Evaluation of myofibroblast inactivation using targeted and nontargeted PI3Ki1 in vitro

To determine whether the nontargeted version of PI3Ki1 might enter HLFs and inhibit PI3K activity, we incubated HLF-FAP cells for 24 hours with either omipalisib or our PI3Ki1 and then examined the impact on TGFβ$_1$ stimulation, including phosphorylation of Akt, collagen synthesis, contraction of a collagen gel, and myofibroblasts apoptosis. As shown in the anti–phospho-Akt blots of Fig. 3A, nontargeted PI3Ki1 inhibited phosphorylation of Akt at least as well as omipalisib, displaying a median inhibitory concentration (IC_{50}) ~1 nM and achieving nearly complete inhibition of Akt phosphorylation on serine-473 ($pAkt^{S473}$) by 10 nM concentration (Fig. 3B). Moreover, nontargeted PI3Ki1 suppressed collagen synthesis with comparable potency to omipalisib, displaying an IC_{50} ~10 nM (Fig. 3C). Quantitation of the ability of PI3Ki1 to inhibit TGFβ$_1$-stimulated fibroblast contraction of a collagen gel further confirmed the ability of PI3Ki1 to reduce TGFβ$_1$-induced collagen remodeling (Fig. 3D). Last, analysis of the impact of nontargeted PI3Ki1 on fibroblast apoptosis (caspases 3 and 7 activation) demonstrated that PI3Ki1 only promoted fibroblast cell death at concentrations much higher than those required to prevent collagen synthesis (Fig. 3E). This weak induction of caspase activity at PI3Ki1 concentrations below 100 nM suggests that a large therapeutic window might exist between PI3Ki1 concentrations required to suppress fibrotic activity and those that cause cell death.

Because many PI3K inhibitors (including omipalisib) exhibit dose-limiting systemic toxicities in humans (*28*–*32*), it became important to determine whether inhibition of PI3K by the FAP-targeted PI3Ki1 conjugate (FAPL-PI3Ki1) might be restricted to FAPL-expressing cells, thereby limiting its toxicity to FAP-expressing cells. We performed three independent experiments as summarized below. First, we stimulated primary lung fibroblasts from a patient with IPF for 24 hours with TGFβ$_1$ (to activate them to a FAP-expressing state; fig. S3) and then incubated the activated fibroblasts for 2 hours with increasing concentrations of FAPL-PI3Ki1, in the presence or absence of 100-fold excess FAPL to block unoccupied FAP sites. As shown in Fig. 4A and fig. S4, phosphorylation of Akt was significantly (200 nM, $P = 0.0074$) inhibited by FAPL-PI3Ki1, and this inhibition was reversed upon coincubation with excess FAPL, demonstrating that FAPL-PI3Ki1 entry into IPF fibroblasts requires an unoccupied FAP on the fibroblast cell

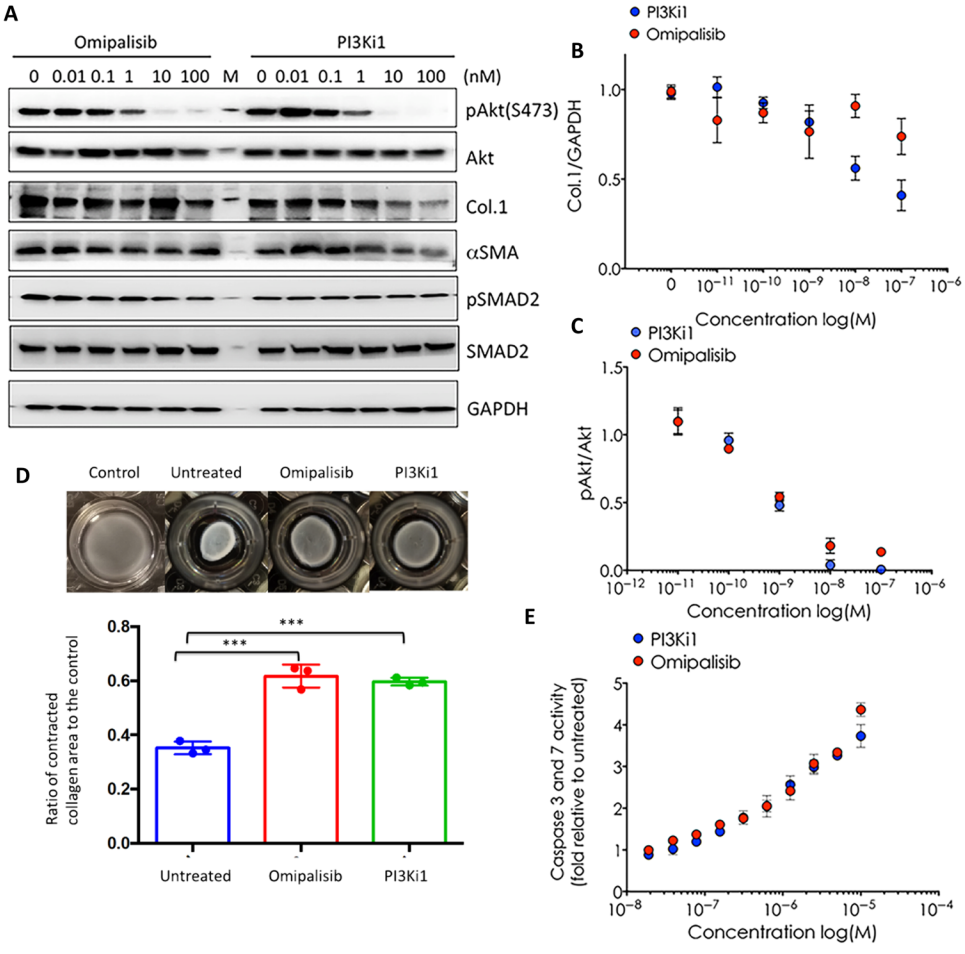

Fig. 3. PI3Ki1 inhibits Akt phosphorylation, collagen synthesis, and collagen gel contraction in human lung fibroblasts (HLFs). (**A**) Confluent HLFs were stimulated with TGFβ_1 (10 ng/ml) and treated with the indicated concentrations of either PI3Ki1 or omipalisib. Lysates were collected and analyzed for the indicated proteins by Western blotting. (**B**) Quantitation of the impact of increasing concentrations of PI3Ki1 or omipalisib on the ratio of phosphorylated Akt (pAkt) to Akt in the same TGFβ_1-stimulated cells. (**C**) Quantitation of the effect of increasing concentrations of PI3Ki1 or omipalisib on the synthesis of collagen 1 by TGFβ_1-stimulated HLF cells. (**D**) Effect of 100 nM PI3Ki1 or omipalisib on the ability of human lung fibroblast to induce contraction of a collagen gel (a characteristic of activated fibroblasts). Data were analyzed using one-way analysis of variance (ANOVA), followed by post hoc Tukey test ($n = 3$; ***$P < 0.001$) (**E**) Effect of increasing concentrations of PI3Ki1 or omipalisib on caspase 3 and 7 activities of HLF cells as a measure of drug-induced apoptosis. The experiments in (A) to (E) have been reproduced three times, each with three independent samples, $n = 3$. No statistical significance was observed for the data presented in (B), (C), or (E).

surface. Second, we stimulated IPF lung fibroblasts with TGFβ_1 and then incubated the cells for different durations with either FAPL-targeted or nontargeted PI3Ki1, followed by replacement of the culture media with inhibitor-free media (Fig. 4B and fig. S4B). Our anticipation was that FAP-targeted PI3Ki1 would be retained by FAP on FAP-expressing cells during short incubation times, whereas nontargeted PI3Ki1 would not be captured by FAP and would subsequently be washed away when the media were changed. As shown in Fig. 4B, FAPL-PI3Ki1 showed a time-dependent reduction in phosphorylated Akt (pAkt), whereas nontargeted PI3Ki1 showed no diminution in pAkt expression up to the longest (81 min) incubation period. Third, FAP involvement in binding and internalization of PI3Ki1 was tested by knocking down FAP in IPF lung fibroblasts using short hairpin RNA (shFAP) and examining the subsequent inhibition of Akt phosphorylation by FAP-PI3Ki1. As seen in Fig. 4 (C and D), shFAP greatly suppresses FAP expression relative to shRNA control–treated IPF lung fibroblasts. Moreover, as shown in Fig. 4C, Akt phosphorylation is visibly less at both 1 and 10 nM FAP-PI3Ki1 in shFAP-treated than shRNA control–treated IPF lung fibroblasts (shCTL). Together, these results suggest that FAP expression is required for uptake and FAPL-PI3Ki1–mediated suppression of TGFβ_1-induced Akt activation in IPF fibroblasts.

Next, we sought to investigate whether our FAP-targeted PI3Ki might suppress collagen formation by human IPF fibroblasts. For this purpose, we incubated the TGFβ_1-stimulated IPF lung fibroblasts for 2 hours with omipalisib, PI3Ki1, or FAPL-PI3Ki1, followed by replacement of the inhibitor-containing media with inhibitor-free growth media and continued incubation for 46 hours. As shown in the collagen-stained micrographs of Fig. 4E and their quantitation in Fig. 4F, incubation with TGFβ_1 was required for stimulation of the biosynthesis of collagen, and this biosynthesis was only moderately inhibited by nontargeted PI3Ki, but strongly ($P < 0.0001$) inhibited by FAP-targeted PI3Ki1. Last, because many PI3Ki exhibit cross-inhibitory activity toward mammalian target of rapamycin (mTOR), we undertook to determine whether FAPL-PI3Ki1 might also suppress phosphorylation of an established substrate of mTOR, namely, 4E-BP1 (*33*). As shown in Fig. 4G, phosphorylation of 4E-BP1 is inhibited by FAPL-PI3Ki1, demonstrating that FAPL-PI3Ki1 inhibits mTOR as well as PI3K. This concurrent suppression of both mTOR and PI3K activity should be very beneficial to the desired therapy because collagen synthesis associated with pathogenic fibrosis can be induced by both pathways (*34*, *35*).

Evaluation of FAPL targeting of a fluorescent dye to fibrotic lung tissue in a mouse model of pulmonary fibrosis

With the promising in vitro results obtained using both an HLF cell line and primary HLFs from a patient with IPF, we sought to investigate the possibility of using FAP to deliver a therapeutic drug to lung myofibroblasts in vivo. For this purpose, we exploited the bleomycin-induced lung fibrosis model in the mouse, in which a single intratracheal instillation of bleomycin (Bleo, 0.75 U/kg) induces pulmonary fibrosis (*36*), including excessive interstitial deposition of collagen, proliferation of several lung cell types, infiltration of immune cells, and contraction of alveolar spaces (fig. S5). To establish

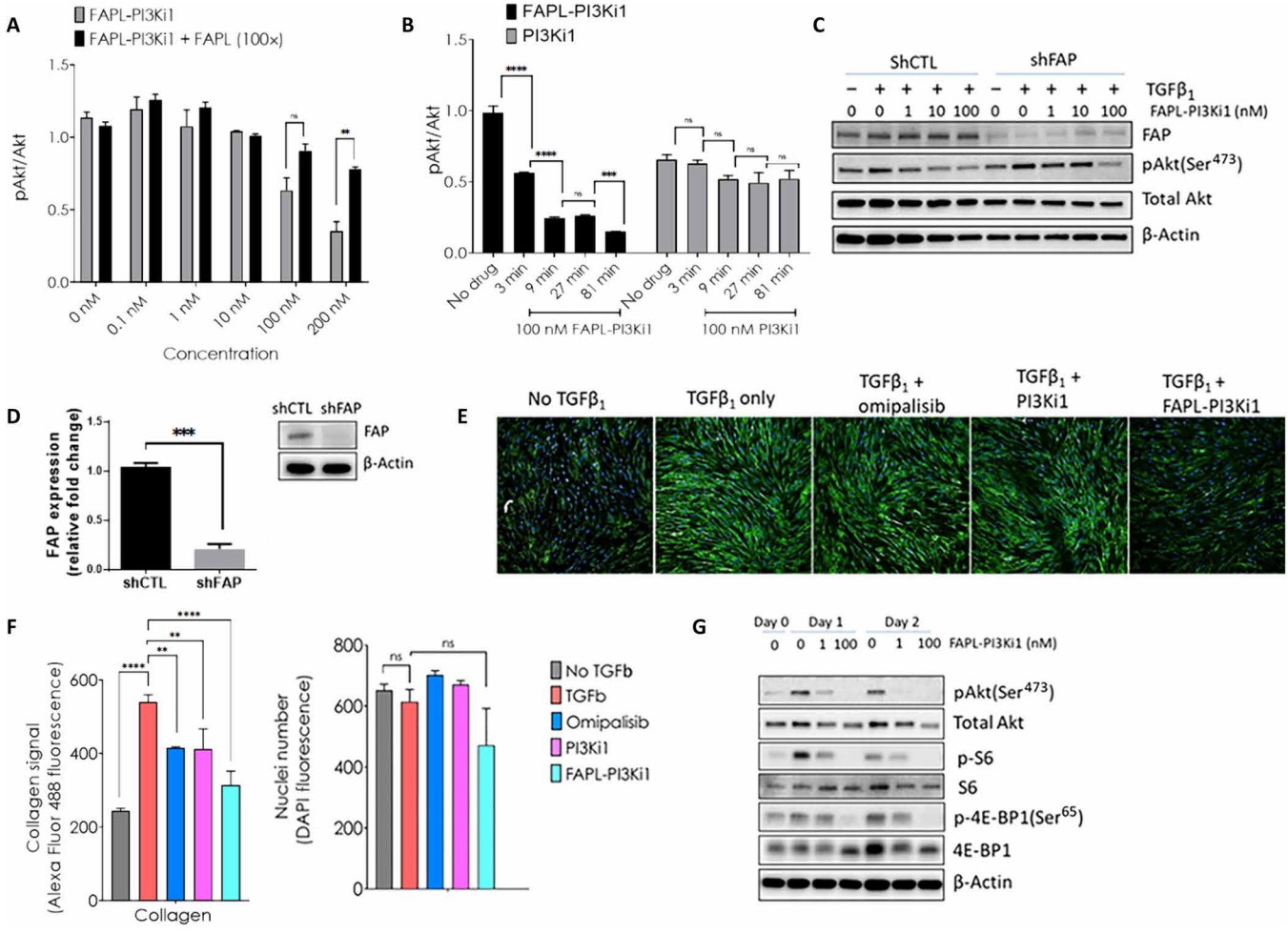

Fig. 4. FAPL-PI3Ki1–induced suppression of TGFβ$_1$-stimulated collagen production and phosphorylation of Akt in IPF fibroblasts requires participation of FAP. (**A**) Confluent human IPF fibroblasts were stimulated with TGFβ$_1$ (10 ng/ml) and then treated with increasing concentrations of FAPL-PI3Ki1 with or without excess FAPL (100×) for 2 hours. After replacing the medium with inhibitor-free medium, the cells were cultured for an additional 22 hours, lysed with phosphatase inhibitor containing cell lysis solution, and analyzed for the indicated proteins by Western blotting (fig. S7A) ($n = 3$). (**B**) Confluent IPF fibroblasts were treated with FAPL-PI3Ki1 or nontargeted PI3Ki1 for 3, 9, 27, or 81 min, after which the media were replaced with TGFβ$_1$ (10 ng/ml) containing media lacking PI3Ki. After an additional 24-hour incubation, cells were lysed and the indicated proteins were analyzed by Western blotting (fig. S7B) ($n = 3$). (**C**) Representative Western blots showing the impact of FAP knockdown with FAP shRNA (shFAP) on the efficiency of FAPL-PI3Ki1 suppression of Akt phosphorylation. Randomized shRNA (shCTL) served as a control ($n = 2$). (**D**) Representative Western blot showing the efficacy of FAP knockdown with FAP-specific and randomized control shRNA in IPF fibroblasts and the densitometric quantification of FAP knockdown in these blots ($n = 3$). (**E** and **F**) Collagen biosynthesis (green channel) was assayed using a molecular crowding assay (0.1% DMSO vehicle was constant for all experimental conditions). IPF fibroblasts were treated with 100 nM omipalisib, PI3Ki1, or FAPL-PI3Ki1 for 2 hours, after which the media were removed and the fibroblasts were further stimulated for 48 hours with media containing TGFβ$_1$ (10 ng/ml). Cell counts were obtained from DAPI counterstaining (blue channel). (**G**) Confluent human IPF fibroblasts were stimulated with TGFβ$_1$ (10 ng/ml) and treated with the indicated concentrations of FAPL-PI3Ki1. Lysates were collected and analyzed for the indicated proteins or phosphoproteins by Western blotting. Akt is a substrate of PI3K, 4E-BP1 is a substrate of mTOR, and *S6* is a substrate of a kinase (*S6* kinase) that is activated by mTOR. Data were analyzed using one-way ANOVA, followed by post hoc Tukey test (**$P < 0.01$, ***$P < 0.001$, ****$P < 0.0001$). ns, not significant.

that this model also results in accumulation of FAP-expressing lung myofibroblasts, we treated Bleo-instilled mice via tail vein injection with 5 nmol of an FAPL-targeted near-infrared (NIR) dye (Fig. 1A, bottom structure; FAPL-S0456) and compared its uptake into affected lungs in the presence and absence of excess FAPL. As shown in Fig. 5A and fig. S6, FAPL-S0456 accumulates specifically in the lungs of Bleo-treated mice, but not in the lungs of healthy mice. Moreover, uptake of FAPL-S0456 in the lungs of Bleo-treated mice can be blocked upon coadministration of excess FAPL, demonstrating that FAPL-S0456 uptake is dependent on both induction of fibrosis and the availability of unoccupied FAP receptors. Evidence that the severity of fibrosis was similar between Bleo-treated control and Bleo-treated competition groups was readily gleaned from data showing a similar amount of hydroxyproline accumulation in both treatment groups (fig. S7). Moreover, in agreement with the known spontaneous resolution of the pathology in this model after day 21 (*37*, *38*) and congruent with the micro computed tomography (micro-CT) data of Fig. 5B, uptake of FAPL-S0456 was absent in the lungs of healthy mice, moderate in the lungs of Bleo-treated mice at day 7 after infusion, prominent in the same mice at day 14 after infusion, and then moderate again in the mice at 21 days after infusion (Fig. 5, C and D). On the basis of these data, we conclude that this

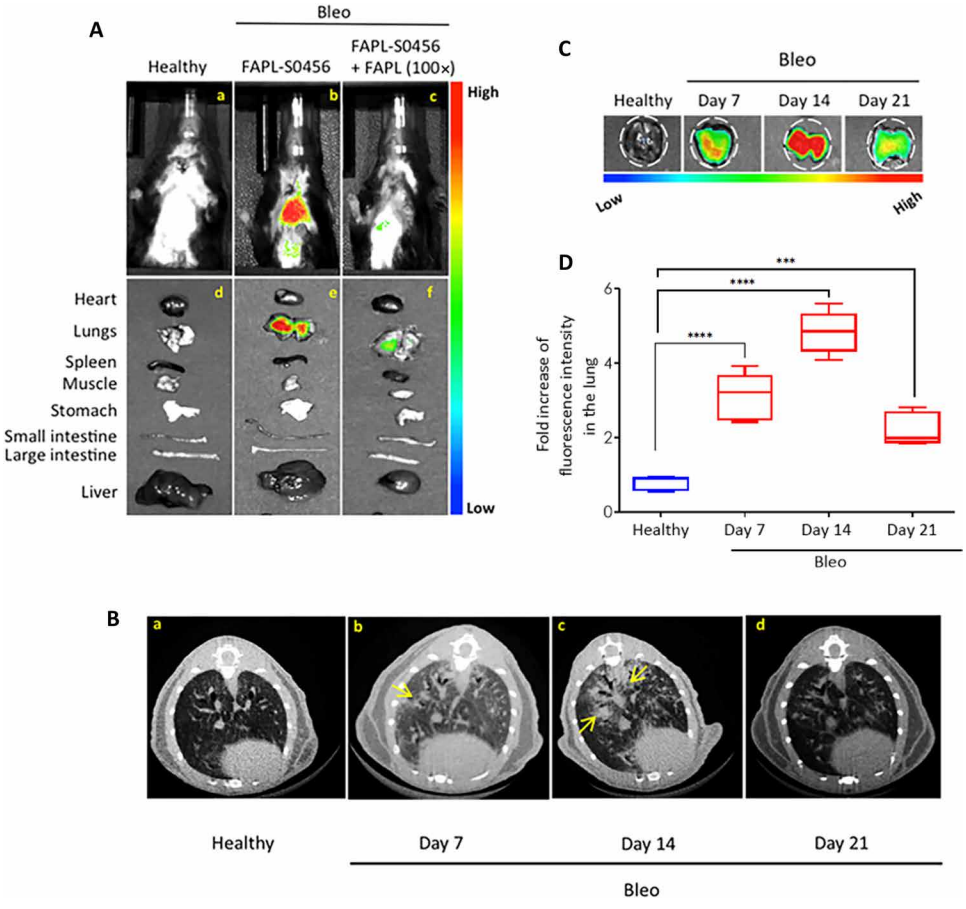

Fig. 5. Optical imaging of bleomycin-induced experimental lung fibrosis in mice with an FAP-targeted NIR dye (FAPL-S0456). (**A**) Representative optical images of whole-body (top) and tissue biodistribution (bottom) of an FAPL-targeted near infrared fluorescent dye (FAPL-S0456) 3 hours after its intravenous administration into mice with Bleo-induced lung fibrosis. Note that little or no FAPL-S0456 is retained in any tissue except the fibrotic lungs, and this lung uptake is both blocked by excess FAPL (right) and absent from healthy mice (left), demonstrating the specificity of FAPL-S0456 for the fibrotic lung. The time course of fibrosis in this model is shown in (**B**) to (**D**). (B) Changes in lung tissue density and bronchiocentric scarring [see arrows in images on days 7 and 14 after intratracheal administration of Bleo (0.75 U/kg)]. (C) Image of lung uptake of FAPL-S0456 over the same time course as in (B) and its quantitation in (D). $n = 5$ for all the groups studied. Data were analyzed using one-way ANOVA, followed by post hoc Tukey test (***$P < 0.0005$, ****$P < 0.0001$).

Bleo-induced fibrosis model in the mouse constitutes a valid system for testing the ability of an FAPL-targeted drug to treat a fibrotic lung disease in vivo.

Evaluation of myofibroblast inactivation after administration of FAP-targeted PI3Ki in vivo

To investigate the therapeutic potential of our fibrosis-targeted PI3Ki1 in vivo, mice were treated with bleomycin as described above and allowed to develop fibrosis before initiation of therapy on day 10 (Fig. 6A). Mice were then injected intravenously (tail vein) every other day with either saline or FAP-PI3Ki1 (2 μmol/kg) and then euthanized on day 21 for analysis of fibrosis. As shown in Fig. 6B, Bleo-treated mice lost weight continuously from the moment of bleomycin instillation, presumably as a consequence of both bleomycin toxicity and progressive fibrosis. In contrast, FAPL-PI3Ki1–treated mice lost weight only until day 12 (until 2 days after initiation of therapy), after which they gained weight continuously. Moreover, all 10 mice that did not receive FAPL-PI3Ki1 died before euthanasia on day 21, whereas only 2 of 10 mice treated with FAPL-PI3Ki1 died before CO_2 euthanasia on day 21 (Fig. 6C). These data suggest that FAPL-PI3Ki1 therapy might affect weight changes and mortality induced by bleomycin.

To obtain more mechanistic information on the molecular basis of the improved survival of the FAPL-PI3Ki1–treated mice, lungs from both saline- and FAPL-PI3Ki1–treated mice were removed and analyzed for hallmarks of lung fibrosis. As shown in Fig. 6D, quantitation of hydroxyproline, a major component of collagen (the dominant biopolymer in fibrosis), was significantly ($P < 0.0001$) elevated in mice treated with saline, but this elevation is significantly ($P < 0.0001$) reduced in mice treated with FAPL-PI3Ki1. This difference in collagen accumulation was confirmed by subjecting thin sections of the lungs to trichrome staining (a stain for collagen), which demonstrated clearly ($P < 0.001$) increased collagen deposition in saline-treated compared with FAPL-PI3Ki1–treated groups (Fig. 6E). More detailed scrutiny of these same thin sections further revealed that the sizes and abundances of air sacs are markedly decreased in saline-treated compared with FAPL-PI3Ki1–exposed cohorts. As shown in Fig. 6 (F to H), evaluation of the lung homogenates from the different groups of mice showed significantly ($P < 0.0112$) reduced αSMA (Fig. 6, F and G) and collagen 1A1 (Fig. 6H) in the FAPL-PI3Ki–treated group. Together, these data demonstrate that administration of a FAP-targeted PI3Ki suppresses the major markers of fibrosis in Bleo-treated mice.

Next, to confirm that the mechanism of FAPL-PI3Ki1 action involves inhibition of PI3K (a major signaling intermediate in the pathway for induction of collagen synthesis), we removed the lungs from Bleo-treated mice 2 hours after intravenous injection of either saline or FAPL-PI3Ki1 and immunoblotted their homogenates with antibodies to Akt and phospho-Akt. As shown in Fig. 6I, treatment with FAPL-PI3Ki1 had no obvious effect on the total amount of Akt (the immediate downstream substrate of PI3K) in the lung homogenates, confirming that the targeted drug is neither eliminating the fibroblasts nor promoting turnover of Akt. In contrast, treatment with FAPL-PI3Ki1 strongly reduced the ratio of pAkt/Akt, the index of protein activation (>95% reduction, $P = 0.0001$; Fig. 6J), confirming that the targeted therapy engages its intended target and thereby blocks the primary signaling pathway for activation of collagen synthesis.

When considered together, the data presented above demonstrate that FAPL-PI3Ki1 suppresses fibrosis in Bleo-treated mice by

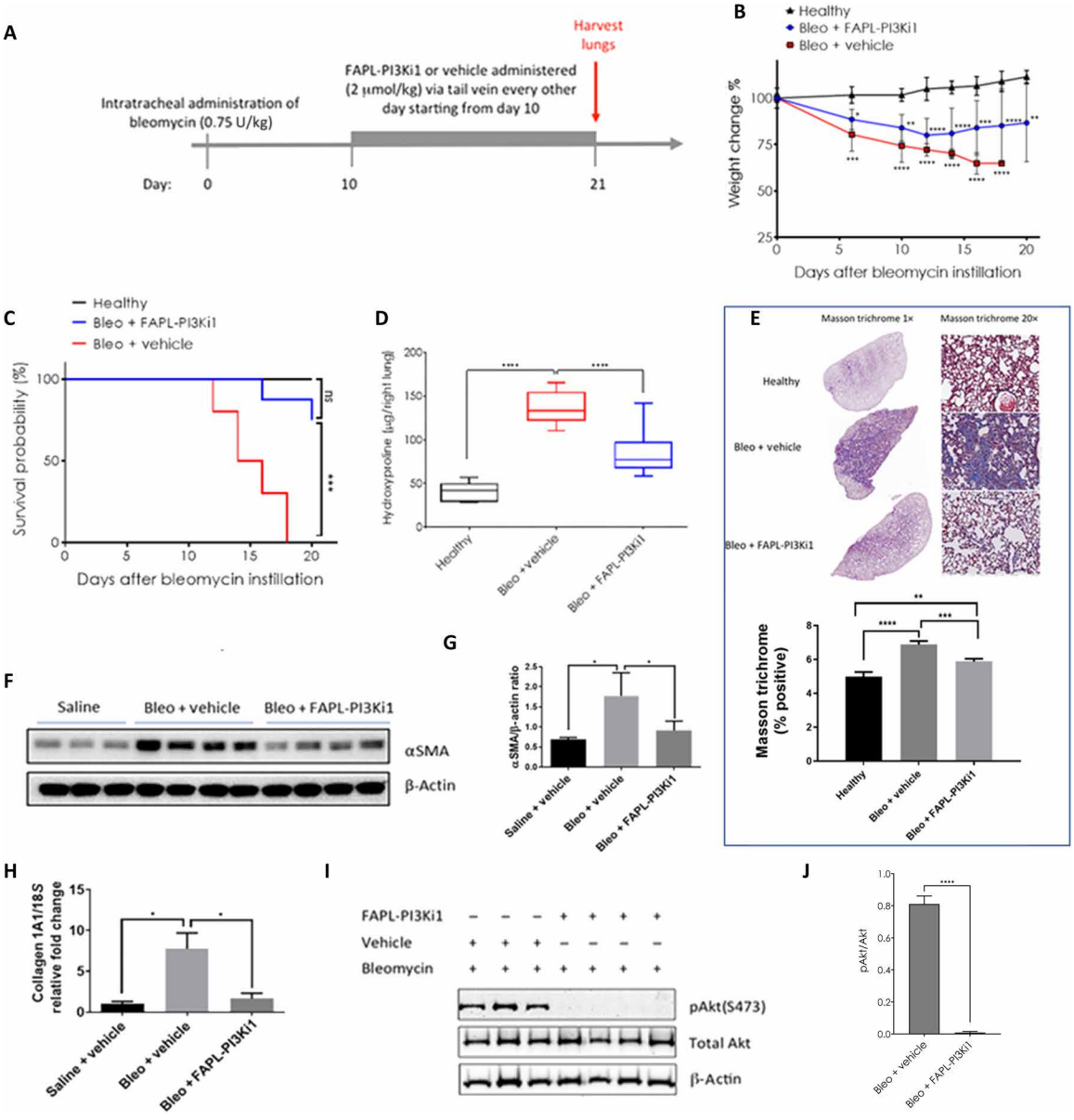

Fig. 6. Evaluation of FAP-targeted PI3K inhibitor (FAPL-PI3Ki1) for treatment of Bleo-induced lung fibrosis in mice. (**A**) Schematic representation of the experimental protocol for induction, treatment, and therapeutic intervention in a bleomycin-induced lung fibrosis model in mice. (**B**) Change in body weight of healthy, FAPL-PI3Ki1–treated (green), and vehicle-treated (red) mice. The body weight changes between Bleo + vehicle group versus healthy group or Bleo + FAPL-PI3Ki1 versus healthy group were analyzed with two-way ANOVA followed by Tukey multiple comparison. *$P < 0.05$, **$P < 0.01$, ***$P < 0.001$, ****$P < 0.0001$. (**C**) Survival of FAPL-PI3Ki1–treated and vehicle-treated mice relative to healthy controls. The survival between Bleo + vehicle group versus healthy group or Bleo + FAPL-PI3Ki1 versus healthy group were analyzed with log-rank (Mantel-Cox) test. ***$P < 0.001$. (**D**) Hydroxyproline content (microgram per right lung) on day 21 of healthy and fibrotic mice after treatment with or without FAPL-PI3Ki1. Hydroxyproline data are displayed as box plots, with the band inside the box representing the mean, and the whiskers representing the minimum and maximum values. (**E**) Masson trichrome staining of excised lung sections from healthy mice and Bleo-treated mice obtained after treatment of FAP-PI3Ki1 or vehicle (control). The data were analyzed using unpaired *t* test comparison (**$P < 0.01$, ***$P < 0.001$, ****$P < 0.0001$). (**F** and **G**) Western blot showing αSMA expression in lungs of different group of mice and densitometric quantification of the αSMA/β-actin ratio. (**H**) Collagen 1A1 expression in lungs of different group of mice. (**I**) Western blot analysis of phosphorylated Akt and total Akt in the lung cell lysates from the contralateral lungs of the same mouse cohorts. (**J**) The ratio of pAkt to Akt in the two different treatment groups. For the pAkt Western blot study, $n = 3$ for the vehicle-treated group, and $n = 4$ for the FAPL-PI3Ki1–treated group. For the different groups in the therapy study, $n = 5$ for the healthy group, $n = 10$ for the FAPL-PI3Ki1 group, and $n = 10$ for the vehicle group. Data in (D), (G), and (H) were analyzed using one-way ANOVA, followed by post hoc Tukey test (*$P < 0.05$). For (J), the data were analyzed using *t* test ($P < 0001$).

inhibiting induction of collagen synthesis via the targeted blockade of PI3K specifically in the fibrotic lungs of affected mice.

FAPL-PI3Ki1 mitigates the TGFβ$_1$-induced profibrotic phenotype and collagen deposition in precision cut lung slices from patients with IPF

Last, to obtain an initial indication of the possible therapeutic benefit that might derive from treatment of human IPF patients with FAPL-PI3Ki1, we prepared precision cut lung slices (PCLS) from resected lungs of patients with IPF and examined the effect of incubation for 72 hours in media containing or lacking 100 nM FAPL-PI3Ki1. As shown in Fig. 7A, incubation with the FAPL-PI3Ki1 strongly ($P < 0.01$) suppressed production of collagen. Moreover, when expression of collagen 1A1 (Fig. 7B) and other markers of fibrosis (fibronectin, Fig. 7C; αSMA, Fig. 7D) was quantitated by quantitative polymerase chain reaction (qPCR), FAPL-PI3Ki1 treatment was confirmed to inhibit transcription of these other hallmarks of fibrosis. Collectively, these data argue that FAPL-PI3Ki1 reduced markers of fibrosis in human samples.

DISCUSSION

Although the causes of fibrosis can be multifarious (*39*), virtually all fibrotic processes seem to involve activation of fibroblasts to myofibroblasts and their subsequent overproduction of collagen (*11*, *40*). On the basis of this commonality and the fact that myofibroblasts are only found in healing wounds (*41*), solid tumors (*17*, *18*, *20*, *21*, *42*), and fibrotic tissues (*15*, *16*, *22*, *23*), it seemed prudent to (i) design a method that would target drugs specifically to myofibroblasts in vivo and then (ii) use the method to deliver collagen synthesis inhibitors selectively to the collagen-synthesizing myofibroblasts. Such a targeted approach should be specific for fibrotic tissue, thereby avoiding any collateral toxicity that might arise when effective drugs are taken up by healthy tissues. Here, we have targeted FAP because this protein is up-regulated whenever a fibroblast is activated to become collagen producing and in some epithelial cells undergoing an epithelial-to-mesenchymal transition (*43*, *44*). We also chose to deliver a PI3Ki because PI3K is central to most pathways involved in induction of collagen synthesis and because a nontargeted PI3Ki is currently undergoing human clinical trials for treatment of IPF (*27*). The fact that FAP-expressing myofibroblasts are critical to the development of IPF (*15*, *45*), our FAPL binds human FAP with high specificity and affinity, and collagen production in primary human IPF lung fibroblasts is potently inhibited by FAPL-PI3Ki1 argue strongly that production of collagen by human myofibroblasts in patients with IPF can also be suppressed by FAPL-PI3Ki1.

Although a number of therapeutic warheads could have been selected for delivery with FAPL, the question naturally arises why a pan PI3Ki was chosen in view of the prior toxicities associated with systemic administration of more isozyme-specific PI3K inhibitors (*46*). The PI3K/Akt/mTOR signaling pathway mediates a variety of critical cellular processes, including cell cycle progression, growth and proliferation, metabolic and synthetic pathways, and a number of inflammatory responses (*25*, *26*, *46*, *47*). Although systemic suppression of these pathways would logically be expected to cause systemic toxicity, when a drug can be targeted to the pathological cell, concerns over systemic toxicities decline because the drug is supposed to specifically target the diseased cells and be excluded by the healthy cells. With this capability, use of a pan PI3Ki could become an advantage because it should avoid problems deriving from leak-through collagen synthesis that arises when minor forms of PI3K become activated.

It has not escaped our notice that bladder fibrosis, cirrhosis of the liver, myelofibrosis, cardiac fibrosis, kidney fibrosis, scleroderma, and other forms of fibrotic disease are all thought to derive from overactivated myofibroblasts that secret more collagen and extracellular matrix proteins than are required for normal tissue repair (*22*, *23*, *48*). Assuming that the myofibroblasts that accumulate in these tissues express FAP and rely on PI3K activation for induction of collagen synthesis (*25*), one might posit that a similar FAP-targeted PI3Ki should prove effective in treating these other forms of fibrosis also. In view of the morbidities and mortality associated with these other fibrotic diseases, it will be important to evaluate similar FAP-targeted

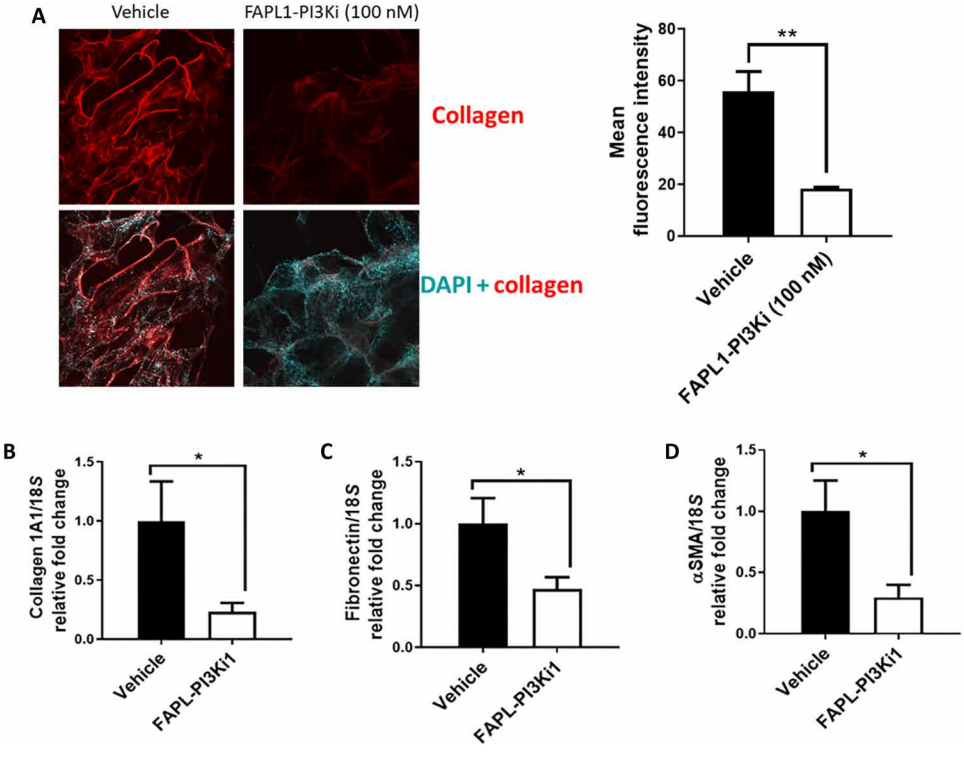

Fig. 7. FAPL-PI3Ki1 reduces profibrotic phenotypes of IPF precision cut lung slices (PCLS). (**A**) Representative collagen (red) and DAPI (blue) staining of PCLS with/without prior treatment with FAPL-PI3Ki1 (100 nM). (**B**) The effect of FAPL-PI3Ki1 on αSMA expression in IPF PCLS. (**C** and **D**) The effect of FAPL-PI3Ki1 on collagen 1A1 and fibronectin expression in IPF PCLS. $N = 6$. *$P < 0.05$, **$P < 0.01$.

fibrosis inhibitors in appropriate animal models to determine whether the same approach might have general applicability. It might also prove useful to develop additional targeting ligands that would enable delivery of drugs to other cells critical to the fibrotic process, such as IPF macrophages that overexpress the beta isoform of the folate receptor (*49*).

Last, although the above targeting strategy shows considerable promise in animal models and human IPF lung slices, one must remember that both murine models and human tissue slices only crudely simulate fibrotic lung conditions in living patients. The effect of FAP-PI3Ki1 on additional animal models and human tissue samples will therefore need to be compared both in the presence and absence of FAP-PI3Ki1 before the conjugate should be considered for preclinical development. It will also be important to perform well-designed pharmacokinetic and pharamacodynamic studies to assure that FAP-PI3Ki1 exhibits the drug-like properties required for the success of a ligand-targeted drug in the clinic.

MATERIALS AND METHODS

Study design

Although PI3K/mTOR inhibitors have been successfully used to inhibit fibrosis in preclinical animal models, no PI3K/mTOR inhibitor has yet been approved for fibrotic applications in humans due to unacceptable off-target toxicities. To determine whether such toxicities could be mitigated by specific targeting of a PI3K/mTOR inhibitor to myofibroblasts (the cells that cause fibrosis), we designed a myofibroblast-targeting ligand and then tested its ability to deliver attached drugs selectively to fibrotic lung myofibroblasts in a bleomycin-induced murine pulmonary fibrosis model. To validate the ability of this targeting ligand to concentrate attached drugs specifically in fibrotic tissue, we first examined its ability to localize a fluorescent dye in the lungs of mice with bleomycin-induced pulmonary fibrosis. We then evaluated the ability of the same targeting ligand to deliver an attached PI3K/mTOR inhibitor to the myofibroblasts of these fibrotic lungs by quantitating the suppression of multiple fibrotic markers. Included among these markers were αSMA (a myofibroblast-specific marker), collagen 1A1, hydroxyproline, fibronectin, the mRNA for αSMA and the mRNA for collagen 1A1. In all cases, the changes in these markers were quantitated in both treated and untreated lungs of bleomycin-induced mice as well as in lungs from healthy mice. To assure statistical significance in all of these studies, preliminary experiments were performed to determine the number of mice per treatment group that would be required to achieve $P < 0.05$ in one-way analysis of variance (ANOVA) tests. These initial studies demonstrated that at least 10 mice per group were needed to achieve statistical significance. Moreover, to assure that the myofibroblast-targeted therapy would address all major symptoms of pulmonary fibrosis, multiple disease-related signal transduction intermediates were monitored to ensure that each major fibrosis pathway would be inhibited by FAP-PI3Ki1. These other fibrosis-related signaling intermediates included phospho-Akt, ribosomal protein *S*6, the transcription factor 4E-BP1, and SMAD2.

All in vitro experiments were performed in triplicate on separate days to ensure reproducibility. In the case of animal studies, mice were randomized according to their body weights before the start of treatments to eliminate any weight-related bias. No samples or animals were ever excluded from data analysis for any reason. In vivo experiments were terminated 21 days after instillation of bleomycin because bleomycin-induced fibrosis is known to begin to resolve spontaneously after that time point (*37*, *38*). All statistical methods are described in the "Statistical analysis" section.

Cell culture and animal husbandry

IPF patient cell lines were obtained from subjects who provided informed consent and underwent lung transplantation, control fibroblasts were obtained from donor organs. C57BL6/6-NCrl (strain code: 027) mice were purchased from Charles River and maintained on normal rodent chow. Mice were housed in a sterile environment on a standard 12-hour light-and-dark cycle for the duration of the study. All animal procedures were approved by the Purdue Animal Care and Use Committee in accordance with the National Institutes of Health guidelines.

Flow cytometry analysis and staining of human lung tissue samples

Human lung tissue samples were obtained from Brigham and Women's Hospital from patients diagnosed with terminal fibrotic lung disease/IPF and required to undergo lung transplants. Control lungs had no evidence of chronic lung disease and/or histological evidence of fibrosis. Tissue digests for flow cytometry were carefully selected by pulmonologists based on biopsy report and CT scans and demonstrated a clear manifestation of the disease of interest. Tissues were initially digested into single-cell suspensions and biobanked in the biorepository. At the time of flow cytometry, single-cell lung digests were thawed in media and placed in phosphate-buffered saline (PBS) containing deoxyribonuclease (DNase) I solution (0.1 mg/ml) (Stem Cell Technologies, catalog no. 07900) to digest DNA from dead cells and prevent cell clumping. Cells were then filtered to remove clumps/debris, counted, and 1 million to 2 million cells were prepared for flow cytometry staining and analysis. Cells were initially stained with a Zombie LIVE/DEAD Viability Dye (BioLegend, catalog no. 423101) in PBS for 30 min at room temperature. Samples were then washed with fluorescence-activated cell sorting (FACS) buffer (0.3% bovine serum albumin in PBS) and stained with Human TruStain FcX (BioLegend, catalog no. 422301) for 15 min to prevent unwanted staining of Fc receptors. Samples were subsequently stained with an antibody cocktail mix in FACS buffer containing anti-human CD45 (APC Fire 750, BioLegend, catalog no. 368518), anti-human CD90/Thy1 (APC, BioLegend, catalog no. 328114), anti-human FAP (PE, R&D Systems, catalog no. FAB3715P), anti-human CD326/EpCAM (PE Cy7, eBioscience, catalog no. 25-9326-42), and anti-human CD144/VE-Cad (BV421, BD Horizon, catalog no. 565671) for 30 min at 4C. Last, samples were washed twice, resuspended in FACS buffer, and examined using a BD LSRFortessa cell analyzer. Data were analyzed using FlowJo version 10.2.

Live cell imaging of FAPL-fluorescein internalization

HLF-hFAP cells were seeded in a glass-bottom dish and incubated overnight with endosome tracker (Rab7a-RFP, Thermo Fisher Scientific). Cells were then incubated with FAPL-fluorescein (10 nM) for 1 hour at 4°C, followed by staining with 5 nM DRAQ5 nuclear dye (Thermo Fisher Scientific). After washing three times in PBS washes, spatial localization of FAPL-fluorescein was monitored at any given time under ambient temperature by confocal microscopy (FV 1000, Olympus). Confocal images were further processed using FV10-ASW Olympus software.

Immunofluorescence of FAP and αSMA expression in fibroblasts

HLF cells, primary human IPF fibroblasts, and non-IPF fibroblasts were cultured, fixed, and permeabilized on glass-bottom dishes for immunofluorescence staining. Primary antibodies against hFAP (1:200; R&D Systems, FAB3715R) or αSMA (1:1000; Abcam, ab21027) were incubated overnight at 4°C. After PBS washes, samples were incubated with Alexa Fluor 488–labeled secondary anti-goat antibodies (1:400; Abcam). Images were captured and analyzed by confocal microscopy.

Western blot analysis of cultured fibroblasts

Serum-starved confluent HLF cells were coincubated in medium containing TGFβ$_1$ (10 ng/ml) with or without the indicated concentrations of PI3K inhibitors for 24 hours. Cells were harvested and lysed for Western blot analysis. After sodium dodecyl sulfate (SDS)–polyacrylamide gel electrophoresis and blocking, membranes were incubated with antibodies to detect pSMAD2$^{Ser465/467}$ (Cell Signaling Technology, #3101) or pAkt^{Ser473} (Cell Signaling Technology, #4060), and signals were visualized with ECL Western Blot Detection Reagents (GE Healthcare). After stripping, membranes were blocked and reprobed with antibodies specific for total SMAD2 (Cell Signaling Technology, #3103) or total Akt (Cell Signaling Technology, #4060).

Molecular crowding assay for collagen

Confluent IPF fibroblasts (4000 cells per well) were cultured in 96-well plates in Dulbecco's modified Eagle's medium (DMEM) containing 0.4% fetal calf serum and ascorbic acid (100 μM), and mixed Ficoll 70 and Ficoll 400 as molecular crowding agents (*25*). Fibroblasts were stimulated with TGFβ$_1$ (10 ng/ml) and incubated with either vehicle [0.1% dimethyl sulfoxide (DMSO)] or 100 nM omipalisib, FAPL-PI3Ki1, or PI3Ki1 for 2 hours, followed by removal of media. Cells were then stimulated with inhibitor-free media containing TGFβ$_1$ (10 ng/ml) for 48 hours. Cells were fixed and stained with antibody specific for human collagen 1 and counterstained with fluorescent secondary antibody (Alex Fluor 488). Nuclei were counterstained with 4′,6-diamidino-2-phenylindole (DAPI) for cell counting on a high content system (Opera Phenix High Content Screening System, PerkinElmer).

Precision cut lung slides

All the procedures were performed under sterile conditions. Bronchoalveolar lavage was performed twice to get rid of any blood coagulation. Prewarmed agarose (Sigma-Aldrich, A0701) was injected to lung explants through the trachea until full inflation. The inflated lung explants were placed on ice for 30 min to solidify the agarose. Tissue cylinder was made using a tissue punch biopsy needle of 10-mm diameter. Lung slides (350 μM) were prepared with VF-300-0Z Vibratome (Precisionary Instruments). The slides were cryopreserved in DMEM with 10% fetal bovine serum and 10% DMSO.

Collagen immunofluorescence staining

PCLSs were put into 24 wells and incubated with MAXblock Blocking Medium (Active Motif) for 1 hour at 37°C. Slides were washed with 1× MAXwash Washing Medium (Active Motif) for 10 min on a rotating platform twice. Primary anti-collagen antibody (Sigma-Aldrich, SAB4200678) was incubated with slides at 1:500 dilution for 1 hour at 37°C. Next, slides were washed with 1× MAXwash Washing Medium (Active Motif) for 10 min on a rotating platform for three times. Second antibody (Sigma-Aldrich, A28180) was diluted at 1:1000 and incubated with slides for 1 hour at 37°C. Slides were washed with 1× MAXwash Washing Medium for 10 min on a rotating platform for five times. Slides were transferred to glass slides and mounted with mounting medium (Sigma-Aldrich, P36934). Images were taken using FLUOVIEW FV10i (Olympus).

Quantitative PCR

RNA was extracted by using TRIzol based on the manufacturer's specification (Invitrogen, 15596026). Extracted RNA was incubated with DNase I (Invitrogen, 18068-015) for 15 min at room temperature followed by DNase I deactivation. Complementary DNA (cDNA) was synthesized by using Superscript IV according to the manufacturer's specification (Invitrogen, 18091050). SYBR Green Supermix was used to perform qPCR (Bio-Rad, 1725121). The primers are listed in the table S2.

Bleomycin-induced lung fibrosis model

Eight- to 10-week-old C57BL/6-NCrl (strain code: 027) male mice (Charles River) were anesthetized (mixture of xylazine/ketamine) and then injected intratracheally with freshly prepared bleomycin sulfate (0.75 U/kg) (Cayman Chemicals, catalog no. 13877) in sterile PBS (volume was varied between 88 and 108 ml depending on the body weight). Control mice were injected with 50 μl of sterile PBS. Body weights were monitored throughout each study. To quantitate FAP expression and fibrosis during longitudinal studies, lungs were harvested at 7, 14, and 21 days after bleomycin instillation and assayed as described below. For therapy studies, induction of IPF was initiated as described above, and drug (2 μmol/kg) was intravenously injected every other day beginning on day 10. Lungs were harvested on day 21 and assayed as described below (day 0 was taken as the day of bleomycin administration).

Western blot analysis of lung tissue

Frozen lungs were lysed in 1 ml of lysis buffer containing a protease inhibitor cocktail using an ULTRA-THURRAX. Lysates were cleared by centrifugation before total protein determination using the BCA protein assay. SDS–polyacrylamide gel electrophoresis and Western blotting were performed following standard procedures. Membranes were blocked and then probed with antibodies directed against glyceraldehyde-3-phosphate dehydrogenase (GAPDH), pAkt, and total Akt. The membranes were then washed in tris-buffered saline/Tween 20 followed by incubation with horseradish peroxidase (HRP)–conjugated secondary antibodies. Immunoreactive bands were detected by addition of an enhanced chemiluminescence substrate.

Immunohistochemistry

Tissue samples were deparaffinized with three changes of xylene, rehydrated in a series of ethanol dilutions (100, 95, and then 70% ethanol) and rinsed well in running distilled water. Antigen retrieval was performed in a pressure cooker for 20 min in Diva Decloaker buffer, and samples were allowed to cool at room temperature for 15 min before washing with distilled water. Slides containing sections were rinsed 2 × 2 min in buffer composed of 50 mM tris (pH 8.4) containing 0.9% sodium chloride and 0.05% Tween 20 (TBST) and blocked with 5% milk in TBST for 60 min at room in a humidified chamber. Sections were rinsed 2 × 2 min in TBST and incubated overnight in a humidified chamber at 4°C with unconjugated AffiniPure Fab fragments of donkey anti-mouse immunoglobulin G (IgG) to

block endogenous mouse IgG background. Sections were rinsed 2 × 2 min in TBST and incubated with primary antibodies for 45 min at room temperature in a humidified chamber followed by 90 min at 4°C. Sections were rinsed 3 × 2 min in TBST and incubated with 3% H_2O_2 in TBST for 10 min to block endogenous peroxidase before another 3 × 2 min rinse in TBST. Slides were incubated with secondary antibody or streptavidin-conjugated HRP at a 1:500 dilution for 20 min at room temperature before a of 3 × 2 min rinse. Detection was carried out using a DAB peroxidase substrate kit following the manufacturer's instructions. Sections were counterstained with Hematoxylin QS for 30 s and rinsed in tap water for 2 min. Samples were dehydrated through graded alcohols, cleared in three changes of xylene, and mounted with permanent mounting media. Sections were imaged and photographed using a Nikon microscope equipped with a DSFi2 camera and analyzed using NIS-Elements software.

Hydroxyproline assay

Total lung collagen was determined by the analysis of hydroxyproline as previously described (*50*). The right lung was consistently set aside for this assay. Briefly, harvested right lung was homogenized in PBS (pH 7.4), and digested with 12 N HCl at 120°C for 3 hours. Citrate/acetate buffer (pH 6.0) and chloramine-T solution were added at room temperature for 20 min, and the samples were incubated with Ehrlich's solution for 15 min at 65°C. Samples were cooled to room temperature and read at 550 nm. Hydroxyproline standards (Sigma-Aldrich) at concentrations between 0 and 400 μg/ml were used to construct a standard curve.

Histopathological evaluation of pulmonary fibrosis

The left lung was inflated and fixed with 10% formalin solution (neutral buffered). Lung tissues were embedded in paraffin, and 10-μm sections were prepared and stained using hematoxylin and eosin and trichrome stain. The severity of bleomycin-induced fibrosis was determined by semiquantitative histopathological scoring at the indicated dates after bleomycin administration (*51*).

In vivo fluorescence imaging

Mice were treated via tail vein injection with 5 nmol of FAP-targeted NIR dye conjugate (FAPL-S0456) and imaged for 2 hours after injection using a Spectral AMI optical imaging system. For competition experiments, a 100-fold excess of the FAP ligand was coadministered with FAPL-S0456. The settings were as follows: object height, 1.5; excitation, 745 nm; emission, 790 nm; field of view (FOV), 25; binning, 2; f-stop, 2; acquisition time, 1 s. After whole-body imaging, animals were dissected, and selected organs were collected and imaged again for complete biodistribution analysis. The conditions remained the same as those used in the longitudinal imaging study, except the mice were imaged on days 7, 14, and 21 after bleomycin administration.

Micro-CT imaging

Micro-CT analysis of whole excised lung was performed on days 7, 14, and 21 after bleomycin administration. Briefly, animals were anesthetized with isoflurane and fixed in prone position. Micro-CT images were acquired on a Quantum FX micro-CT system (Perkin Elmer) with cardiac gating (without respiratory gating), using the following parameters: 90 kV; 160 μA; FOV, 60 × 60 × 60 mm; spatial resolution, 0.11 mm, resulting in a total acquisition time of 4 to 5 min.

Pharmacokinetic analysis

FAPL-PI3Ki1 (2 μmol/kg) was intravenously injected into healthy C57BL/6-NCrl mice, and blood was collected at 5, 10, 15, 20, 25, 30, 60, 120, 180, 240, and 300 min after injection. Samples were centrifuged at 1000*g* for 10 min, and plasma was collected and treated with acetonitrile [plasma/acetonitrile = 1/3 (v/v)]. After vortexing and then centrifuging at 1000*g* for 5 min, the supernatant was collected and injected into an Agilent 6410 NanoLC QQQ liquid chromatography–mass spectrometry for quantitation of FAPL-PI3Ki1 concentration. Column: Agilent Eclipse Plus C18, 2.1 × 50 mm; SN: B17477. Eluent: A, water + 0.1% formic acid; B, acetonitrile + 0.1% formic acid. The pharmacokinetic data are reported in fig. S9A.

Stability analysis

Ten microliters of 5 mM FAPL-PI3Ki1 was added to 100 μl of plasma obtained from healthy C57BL/6-NCrl mice and incubated at 37°C for 3, 5, 10, 15, 20, 30, 40, 50, 60, 90, or 120 min. Samples were then extracted with acetonitrile and analyzed as described above. The concentration of FAPL-PI3Ki1 and PI3Ki1 as a function of time is shown in fig. S9B.

Cell viability assay

Cell viability was measured by MTT assay (fig. S9). Briefly, (3-(4,5-dimethylthiazol2-yl)-2,5-diphenyltetrazolium bromide) (Sigma-Aldrich, M2003-1g) was dissolved in sterile PBS to make a stock solution at 5 mg/ml. To measure cell viability, MTT solution was added to cell culture medium and incubated with cell for 1 hour at 37°C. DMSO was used to dissolve the formazan and then measured at OD590 (optical density at 590 nM) using a BioTek EPOCH microplate reader.

Statistical analysis

Data are presented as mean ± SEM or ±SD as denoted in the figure legends. Statistical differences were assessed using *t* test with GraphPad Prism software. Kaplan-Meier survival curves were used to compare mortality, and log-rank testing was used to assess differences in survival. A one-way ANOVA followed by post hoc Tukey test was used for analyzing differences between treatment groups. Asterisks indicate statistically significant differences (*$P < 0.05$, **$P < 0.01$, ***$P < 0.001$, ****$P < 0.0001$).

SUPPLEMENTARY MATERIALS

stm.sciencemag.org/cgi/content/full/12/567/eaay3724/DC1

Fig. S1. Flow cytometric analysis of human lung tissue samples showing up-regulation of FAP on IPF lung fibroblasts.
Fig. S2. Binding of FAPL-fluorescein to HLF cells before (red dots) and after (blue dots) transfection with human FAP.
Fig. S3. TGFβ_1 induced FAP and αSMA expression in an HLF cell line.
Fig. S4. FAP-targeted PI3Ki (FAPL-PI3Ki1) suppresses phosphorylation of Akt in IPF fibroblasts.
Fig. S5. Characterization of the time course of development of pulmonary fibrosis after intratracheal administration of bleomycin (0.75 U/kg) to mice.
Fig. S6. Quantitative biodistribution of FAPL_S0456 in healthy and bleomycin-treated mice.
Fig. S7. Quantification of optical imaging of bleomycin-induced experimental lung fibrosis in mice with a FAP-targeted NIR dye (FAPL-S0456).
Fig. S8. Hydroxyproline content in the lungs of bleomycin-treated mice receiving FAPL-S0456 in either the presence or absence of excess FAPL (100×).
Fig. S9. Analysis of pharmacokinetics and stability of FAPL-PI3Ki1.
Fig. S10. Evaluation of HLF survival (MTT assay).
Table S1. Docking and docking glide-score for the compounds docked in the active site of PI3Kγ (PDB code: 3L08) using Schrödinger Maestro software.
Table S2. Primer sequence.

Data file S1. Raw data.
Data file S2. Synthetic procedures and schemes.

View/request a protocol for this paper from *Bio-protocol*.

REFERENCES AND NOTES

1. D. Lagares, O. Busnadiego, R. A. García-Fernández, M. Kapoor, S. Liu, D. E. Carter, D. Abraham, X. Shi-Wen, P. Carreira, B. A. Fontaine, B. S. Shea, A. M. Tager, A. Leask, S. Lamas, F. Rodríguez-Pascual, Inhibition of focal adhesion kinase prevents experimental lung fibrosis and myofibroblast formation. *Arthritis Rheum.* **64**, 1653–1664 (2012).
2. S. L. Friedman, D. Sheppard, J. S. Duffield, S. Violette, Therapy for fibrotic diseases: Nearing the starting line. *Sci. Transl. Med.* **5**, 167sr1 (2013).
3. C. B. Nanthakumar, R. J. D. Hatley, S. Lemma, J. Gauldie, R. P. Marshall, S. J. F. MacDonald, Dissecting fibrosis: Therapeutic insights from the small-molecule toolbox. *Nat. Rev. Drug Discov.* **14**, 693–720 (2015).
4. M. Baues, A. Dasgupta, J. Ehling, J. Prakash, P. Boor, F. Tacke, F. Kiessling, T. Lammers, Fibrosis imaging: Current concepts and future directions. *Adv. Drug Deliv. Rev.* **121**, 9–26 (2017).
5. Anon, At the frontiers of lung fibrosis therapy. *Nat. Biotechnol.* **31**, 781–783 (2013).
6. Y.-M. Liu, K. Nepali, J.-P. Liou, Idiopathic pulmonary fibrosis: Current status, recent progress, and emerging targets. *J. Med. Chem.* **60**, 527–553 (2017).
7. S.-M. Koo, S.-T. Uh, D. S. Kim, Y. W. Kim, M. P. Chung, C. S. Park, S. H. Jeong, Y. B. Park, H. L. Lee, J. W. Shin, E. J. Lee, J. H. Lee, Y. Jegal, H. K. Lee, Y. H. Kim, J. W. Song, M. S. Park, Y. Hwangbo, Relationship between survival and age in patients with idiopathic pulmonary fibrosis. *J. Thorac. Dis.* **8**, 3255–3264 (2016).
8. E. Fernández Fabrellas, R. Peris Sánchez, C. Sabater Abad, G. Juan Samper, Prognosis and follow-up of idiopathic pulmonary fibrosis. *Med. Sci. (Basel)* **6**, 51 (2018).
9. S. D. Knight, N. D. Adams, J. L. Burgess, A. M. Chaudhari, M. G. Darcy, C. A. Donatelli, J. I. Luengo, K. A. Newlander, C. A. Parrish, L. H. Ridgers, M. A. Sarpong, S. J. Schmidt, G. S. Van Aller, J. D. Carson, M. A. Diamond, P. A. Elkins, C. M. Gardiner, E. Garver, S. A. Gilbert, R. R. Gontarek, J. R. Jackson, K. L. Kershner, L. Luo, K. Raha, C. S. Sherk, C.-M. Sung, D. Sutton, P. J. Tummino, R. J. Wegrzyn, K. R. Auger, D. Dhanak, Discovery of GSK2126458, a highly potent inhibitor of PI3K and the mammalian target of rapamycin. *ACS Med. Chem. Lett.* **1**, 39–43 (2010).
10. J. C. Bendell, A. M. Varghese, D. M. Hyman, T. M. Bauer, S. Pant, S. Callies, J. Lin, R. Martinez, E. Wickremsinhe, A. Fink, V. Wacheck, K. N. Moore, A first-in-human phase 1 study of LY3023414, an oral PI3K/mTOR dual inhibitor, in patients with advanced cancer. *Clin. Cancer Res.* **24**, 3253–3262 (2018).
11. M. W. Moore, E. L. Herzog, Regulation and relevance of myofibroblast responses in idiopathic pulmonary fibrosis. *Curr. Pathobiol. Rep.* **1**, 199–208 (2013).
12. V. J. Thannickal, D. Y. Lee, E. S. White, Z. Cui, J. M. Larios, R. Chacon, J. C. Horowitz, R. M. Day, P. E. Thomas, Myofibroblast differentiation by transforming growth factor-β1 is dependent on cell adhesion and integrin signaling via focal adhesion kinase. *J. Biol. Chem.* **278**, 12384–12389 (2003).
13. P.-S. Bellaye, C. Shimbori, C. Upagupta, S. Sato, W. Shi, J. Gauldie, K. Ask, M. Kolb, Lysyl oxidase–like 1 protein deficiency protects mice from adenoviral transforming growth factor-β1–induced pulmonary fibrosis. *Am. J. Respir. Cell Mol. Biol.* **58**, 461–470 (2018).
14. E. S. White, Lung extracellular matrix and fibroblast function. *Ann. Am. Thorac. Soc.* **12**, S30–S33 (2015).
15. P. S. Acharya, A. Zukas, V. Chandan, A.-L. A. Katzenstein, E. Puré, Fibroblast activation protein: A serine protease expressed at the remodeling interface in idiopathic pulmonary fibrosis. *Hum. Pathol.* **37**, 352–360 (2006).
16. J. Niedermeyer, P. Garin-Chesa, M. Kriz, F. Hilberg, E. Mueller, U. Bamberger, W. J. Rettig, A. Schnapp, Expression of the fibroblast activation protein during mouse embryo development. *Int. J. Dev. Biol.* **45**, 445–447 (2001).
17. J. E. Park, M. C. Lenter, R. N. Zimmermann, P. Garin-Chesa, L. J. Old, W. J. Rettig, Fibroblast activation protein, a dual specificity serine protease expressed in reactive human tumor stromal fibroblasts. *J. Biol. Chem.* **274**, 36505–36512 (1999).
18. M. J. Scanlan, B. K. Raj, B. Calvo, P. Garin-Chesa, M. P. Sanz-Moncasi, J. H. Healey, L. J. Old, W. J. Rettig, Molecular cloning of fibroblast activation protein alpha, a member of the serine protease family selectively expressed in stromal fibroblasts of epithelial cancers. *Proc. Natl. Acad. Sci. U.S.A.* **91**, 5657–5661 (1994).
19. M. Jacob, L. Chang, E. Puré, Fibroblast activation protein in remodeling tissues. *Curr. Mol. Med.* **12**, 1220–1243 (2012).
20. W. N. Brennen, J. T. Isaacs, S. R. Denmeade, Rationale behind targeting fibroblast activation protein-expressing carcinoma-associated fibroblasts as a novel chemotherapeutic strategy. *Mol. Cancer Ther.* **11**, 257–266 (2012).
21. S. J. Cohen, R. K. Alpaugh, I. Palazzo, N. J. Meropol, A. Rogatko, Z. Xu, J. P. Hoffman, L. M. Weiner, J. D. Cheng, Fibroblast activation protein and its relationship to clinical outcome in pancreatic adenocarcinoma. *Pancreas* **37**, 154–158 (2008).
22. M. T. Levy, G. W. McCaughan, C. A. Abbott, J. E. Park, A. M. Cunningham, E. Müller, W. J. Rettig, M. D. Gorrell, Fibroblast activation protein: A cell surface dipeptidyl peptidase and gelatinase expressed by stellate cells at the tissue remodelling interface in human cirrhosis. *Hepatology* **29**, 1768–1778 (1999).
23. X. M. Wang, T.-W. Yao, N. A. Nadvi, B. Osborne, G. W. McCaughan, M. D. Gorrell, Fibroblast activation protein and chronic liver disease. *Front. Biosci.* **13**, 3168–3180 (2008).
24. J. Roy, S. U. Hettiarachchi, M. Kaake, R. Mukkamala, P. S. Low, Design and validation of fibroblast activation protein alpha targeted imaging and therapeutic agents. *Theranostics* **10**, 5778–5789 (2020).
25. P. F. Mercer, H. V. Woodcock, J. D. Eley, M. Platé, M. G. Sulikowski, P. F. Durrenberger, L. Franklin, C. B. Nanthakumar, Y. Man, F. Genovese, R. J. McAnulty, S. Yang, T. M. Maher, A. G. Nicholson, A. D. Blanchard, R. P. Marshall, P. T. Lukey, R. C. Chambers, Exploration of a potent PI3 kinase/mTOR inhibitor as a novel anti-fibrotic agent in IPF. *Thorax* **71**, 701–711 (2016).
26. C. E. Winbanks, L. Grimwood, A. Gasser, I. A. Darby, T. D. Hewitson, G. J. Becker, Role of the phosphatidylinositol 3-kinase and mTOR pathways in the regulation of renal fibroblast function and differentiation. *Int. J. Biochem. Cell Biol.* **39**, 206–219 (2007).
27. P. T. Lukey, S. A. Harrison, S. Yang, Y. Man, B. F. Holman, A. Rashidnasab, G. Azzopardi, M. Grayer, J. K. Simpson, P. Bareille, L. Paul, H. V. Woodcock, R. Toshner, P. Saunders, P. L. Molyneaux, K. Thielemans, F. J. Wilson, P. F. Mercer, R. C. Chambers, A. M. Groves, W. A. Fahy, R. P. Marshall, T. M. Maher, A randomised, placebo-controlled study of omipalisib (PI3K/mTOR) in idiopathic pulmonary fibrosis. *Eur. Respir. J.* **53**, 1801992 (2019).
28. J. E. Grilley-Olson, P. L. Bedard, A. Fasolo, M. Cornfeld, L. Cartee, A. R. Abdul Razak, L.-A. Stayner, Y. Wu, R. Greenwood, R. Singh, C. B. Lee, J. Bendell, H. A. Burris, G. Del Conte, C. Sessa, J. R. Infante, A phase Ib dose-escalation study of the MEK inhibitor trametinib in combination with the PI3K/mTOR inhibitor GSK2126458 in patients with advanced solid tumors. *Invest. New Drugs* **34**, 740–749 (2016).
29. P. Munster, R. Aggarwal, D. Hong, J. H. M. Schellens, R. van der Noll, J. Specht, P. O. Witteveen, T. L. Werner, E. C. Dees, E. Bergsland, N. Agarwal, J. F. Kleha, M. Durante, L. Adams, D. A. Smith, T. A. Lampkin, S. R. Morris, R. Kurzrock, First-in-human phase I study of GSK2126458, an oral pan-class I phosphatidylinositol-3-kinase inhibitor, in patients with advanced solid tumor malignancies. *Clin. Cancer Res.* **22**, 1932–1939 (2016).
30. P. A. Jänne, R. B. Cohen, A. D. Laird, S. Macé, J. A. Engelman, R. Ruiz-Soto, K. Rockich, J. Xu, G. I. Shapiro, P. Martinez, E. Felip, Phase I safety and pharmacokinetic study of the PI3K/mTOR inhibitor SAR245409 (XL765) in combination with erlotinib in patients with advanced solid tumors. *J. Thorac. Oncol.* **9**, 316–323 (2014).
31. J. M. del Campo, M. Birrer, C. Davis, K. Fujiwara, A. Gollerkeri, M. Gore, B. Houk, S. Lau, A. Poveda, A. González-Martín, C. Muller, K. Muro, K. Pierce, M. Suzuki, J. Vermette, A. Oza, A randomized phase II non-comparative study of PF-04691502 and gedatolisib (PF-05212384) in patients with recurrent endometrial cancer. *Gynecol. Oncol.* **142**, 62–69 (2016).
32. Z. A. Wainberg, M. Alsina, H. P. Soares, I. Braña, C. D. Britten, G. D. Conte, P. Ezeh, B. Houk, K. A. Kern, S. Leong, N. Pathan, K. J. Pierce, L. L. Siu, J. Vermette, J. Tabernero, A multi-arm phase I study of the PI3K/mTOR inhibitors PF-04691502 and gedatolisib (PF-05212384) plus irinotecan or the MEK inhibitor PD-0325901 in advanced cancer. *Target. Oncol.* **12**, 775–785 (2017).
33. H. V. Woodcock, J. D. Eley, D. Guillotin, M. Platé, C. B. Nanthakumar, M. Martufi, S. Peace, G. Joberty, D. Poeckel, R. B. Good, A. R. Taylor, N. Zinn, M. Redding, E. J. Forty, R. E. Hynds, C. Swanton, M. Karsdal, T. M. Maher, A. Fisher, G. Bergamini, R. P. Marshall, A. D. Blanchard, P. F. Mercer, R. C. Chambers, The mTORC1/4E-BP1 axis represents a critical signaling node during fibrogenesis. *Nat. Commun.* **10**, 6 (2019).
34. X.-L. Zhang, R.-G. Xing, L. Chen, C.-R. Liu, Z.-G. Miao, PI3K/Akt signaling is involved in the pathogenesis of bleomycin induced pulmonary fibrosis via regulation of epithelial mesenchymal transition. *Mol. Med. Rep.* **14**, 5699–5706 (2016).
35. J. B. Kral, M. Kuttke, W. C. Schrottmaier, B. Birnecker, J. Warszawska, C. Wernig, H. Paar, M. Salzmann, E. Sahin, J. S. Brunner, C. Österreicher, S. Knapp, A. Assinger, G. Schabbauer, Sustained PI3K activation exacerbates BLM-induced lung fibrosis via activation of pro-inflammatory and pro-fibrotic pathways. *Sci. Rep.* **6**, 23034 (2016).
36. D. M. Walters, S. R. Kleeberger, Mouse models of bleomycin-induced pulmonary fibrosis. *Curr. Protoc. Pharmacol.* **40**, 5.46.1–5.46.17 (2008).
37. B. B. Moore, W. E. Lawson, T. D. Oury, T. H. Sisson, K. Raghavendran, C. M. Hogaboam, Animal models of fibrotic lung disease. *Am. J. Respir. Cell Mol. Biol.* **49**, 167–179 (2013).
38. J. Tashiro, G. A. Rubio, A. H. Limper, K. Williams, S. J. Elliot, I. Ninou, V. Aidinis, A. Tzouvelekis, M. K. Glassberg, Exploring animal models that resemble idiopathic pulmonary fibrosis. *Front. Med. (Lausanne)* **4**, 118 (2017).
39. S. W. Glasser, J. S. Hagood, S. Wong, C. A. Taype, S. K. Madala, W. D. Hardie, Mechanisms of lung fibrosis resolution. *Am. J. Pathol.* **186**, 1066–1077 (2016).
40. T. A. Wynn, T. R. Ramalingam, Mechanisms of fibrosis: Therapeutic translation for fibrotic disease. *Nat. Med.* **18**, 1028–1040 (2012).
41. S. Mathew, M. J. Scanlan, B. K. M. Raj, V. V. V. S. Murty, P. Garin-Chesa, L. J. Old, W. J. Rettig, R. S. K. Chaganti, The gene for fibroblast activation protein α (*FAP*), a putative cell surface-bound serine protease expressed in cancer stroma and wound healing, maps to chromosome band 2q23. *Genomics* **25**, 335–337 (1995).

42. W. L. Monsky, C.-Y. Lin, A. Aoyama, T. Kelly, S. K. Akiyama, S. C. Mueller, W.-T. Chen, A potential marker protease of invasiveness, seprase, is localized on invadopodia of human malignant melanoma cells. *Cancer Res.* **54**, 5702–5710 (1994).
43. S. Yazdani, R. Bansal, J. Prakash, Drug targeting to myofibroblasts: Implications for fibrosis and cancer. *Adv. Drug Deliv. Rev.* **121**, 101–116 (2017).
44. Z. Kahounová, D. Kurfürstová, J. Bouchal, G. Kharaishvili, J. Navrátil, J. Remšík, Š. Šimečková, V. Študent, A. Kozubík, K. Souček, The fibroblast surface markers FAP, anti-fibroblast, and FSP are expressed by cells of epithelial origin and may be altered during epithelial-to-mesenchymal transition. *Cytometry A* **93**, 941–951 (2018).
45. C. Egger, C. Cannet, C. Gérard, T. Suply, I. Ksiazek, E. Jarman, N. Beckmann, Effects of the fibroblast activation protein inhibitor, PT100, in a murine model of pulmonary fibrosis. *Eur. J. Pharmacol.* **809**, 64–72 (2017).
46. R. Dienstmann, J. Rodon, V. Serra, J. Tabernero, Picking the point of inhibition: A comparative review of PI3K/AKT/mTOR pathway inhibitors. *Mol. Cancer Ther.* **13**, 1021–1031 (2014).
47. R. Reilly, M. S. Mroz, E. Dempsey, K. Wynne, S. J. Keely, E. F. McKone, C. Hiebel, C. Behl, J. A. Coppinger, Targeting the PI3K/Akt/mTOR signalling pathway in cystic fibrosis. *Sci. Rep.* **7**, 7642 (2017).
48. Y. Liu, Renal fibrosis: New insights into the pathogenesis and therapeutics. *Kidney Int.* **69**, 213–217 (2006).
49. L. E. Kelderhouse, M. T. Robins, K. E. Rosenbalm, E. K. Hoylman, S. Mahalingam, P. S. Low, Prediction of response to therapy for autoimmune/inflammatory diseases using an activated macrophage-targeted radioimaging agent. *Mol. Pharm.* **12**, 3547–3555 (2015).
50. B. B. Moore, R. Paine III, P. J. Christensen, T. A. Moore, S. Sitterding, R. Ngan, C. A. Wilke, W. A. Kuziel, G. B. Toews, Protection from pulmonary fibrosis in the absence of CCR2 signaling. *J. Immunol.* **167**, 4368–4377 (2001).
51. T. Ashcroft, J. M. Simpson, V. Timbrell, Simple method of estimating severity of pulmonary fibrosis on a numerical scale. *J. Clin. Pathol.* **41**, 467–470 (1988).

Acknowledgments: We thank V. A. Bernal-Crespo and the core of Purdue Histology Research Laboratory for work on mice lung tissue samples. **Funding:** This study was supported by a gift from the Hurvis Charitable Foundation to P.S.L. **Author contributions:** P.S.L. conceived of the project and supervised the general design of the study. S.U.H., Y.-H.L., F.Z., E.P.-C., K.T., X.L., E.A.A., C.N.-N., M.S., I.O.R., and P.S.L. designed the experiments. J.R. developed the targeting ligand, and S.U.H. developed the PI3Ki1. S.U.H. and S.D.L. synthesized and characterized the many different conjugates reported in the paper. S.U.H., F.Z., E.P.-C., Y.-H.L., S.D.L., K.T., and X.L. performed the animal experiments. S.U.H., Y.-H.L., X.L., and P.S.L. analyzed the data. I.O.R., K.T., and X.L. worked with IPF patient PCLS. S.U.H., Y.-H.L., and X.L. performed all the in vitro experiments. S.U.H. and P.S.L. wrote the manuscript draft, which was then further refined by I.O.R. and P.S.L. All other authors reviewed and edited the intermediate and final versions of the manuscript. **Competing interests:** The authors declare that they have no competing financial interests. The technology disclosed in this paper has been patented [(Fibroblast activation protein (FAP) targeted imaging and therapy in fibrosis, PCT/US19/56257]. **Data and materials availability:** All data associated with this study are present in the paper or the Supplementary Materials.

Submitted 14 June 2019
Resubmitted 24 November 2019
Accepted 29 June 2020
Published 28 October 2020
10.1126/scitranslmed.aay3724

Citation: S. U. Hettiarachchi, Y.-H. Li, J. Roy, F. Zhang, E. Puchulu-Campanella, S. D. Lindeman, M. Srinivasarao, K. Tsoyi, X. Liang, E. A. Ayaub, C. Nickerson-Nutter, I. O. Rosas, P. S. Low, Targeted inhibition of PI3 kinase/mTOR specifically in fibrotic lung fibroblasts suppresses pulmonary fibrosis in experimental models. *Sci. Transl. Med.* **12**, eaay3724 (2020).

Science Translational Medicine

Targeted inhibition of PI3 kinase/mTOR specifically in fibrotic lung fibroblasts suppresses pulmonary fibrosis in experimental models

Suraj U. Hettiarachchi, Yen-Hsing Li, Jyoti Roy, Fenghua Zhang, Estela Puchulu-Campanella, Spencer D. Lindeman, Madduri Srinivasarao, Konstantin Tsoyi, Xiaoliang Liang, Ehab A. Ayaub, Cheryl Nickerson-Nutter, Ivan O. Rosas and Philip S. Low

Sci Transl Med **12**, eaay3724.
DOI: 10.1126/scitranslmed.aay3724

Mitigating collagen production

Idiopathic pulmonary fibrosis (IPF) is characterized by deposition of collagen in the lung parenchyma by activated myofibroblasts, cell type exclusively expressing fibroblast activation protein (FAP). Now, Hettiarachchi *et al.* took advantage of this property and developed a low-molecular weight FAP agonist that could be used to deliver therapeutics to fibrotic tissue. A FAP-targeted phosphatidylinositol 3-kinase (PI3K) inhibitor was shown to reduce collagen production in human IPF lung fibroblasts and had therapeutic effects in a mouse model of IPF. The results suggest that FAP-targeting therapeutics could be effective for treating IPF.